Final report
OTKA K 116036 project

November 2021

Participants – *PI:*

Ellák Somfai

Senior researchers:

Tamás Börzsönyi
János Török

Junior researchers:

Balázs Szabó
Dániel Nagy
Sára Lévay
Viktor Nagy
Tivadar Pongó

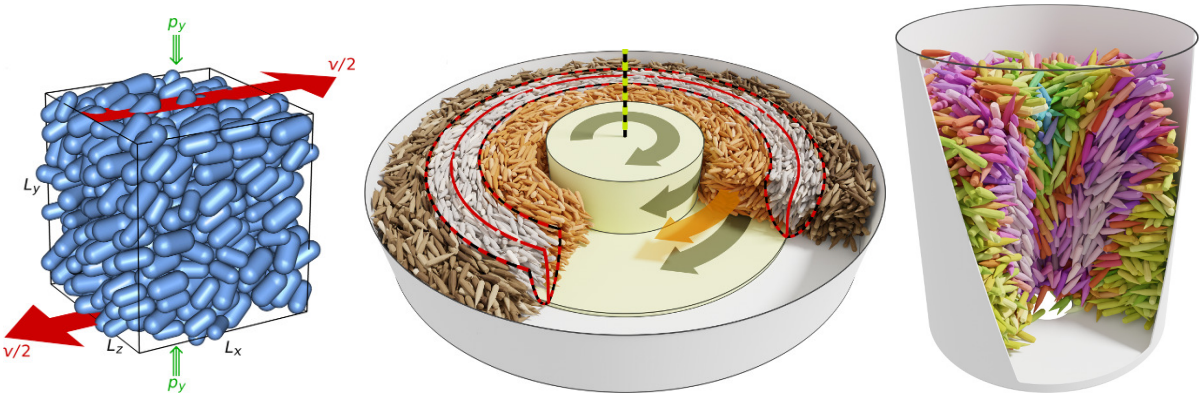

Representative geometries of experiments and numerical modelling of elongated granular asemblies – from left to right: plane Couette, cylindrical split bottom shear cell, silo (hopper).

In this document we provide a scientific summary of the project.

Rheology of dry granular assemblies of elongated particles

As a first highlight, we present our results on the rheology of dense granular flows made up of elongated particles. The established theory for granular rheology is the $\mu(I)$ framework: its central quantity is the effective friction μ, describing the ratio of the shear stress to the pressure in response to shear deformations. We were interested in the rheological properties of granular packing made up of elongated particles, as the shear induced ordering observed earlier in such systems is expected to influence the rheological properties.

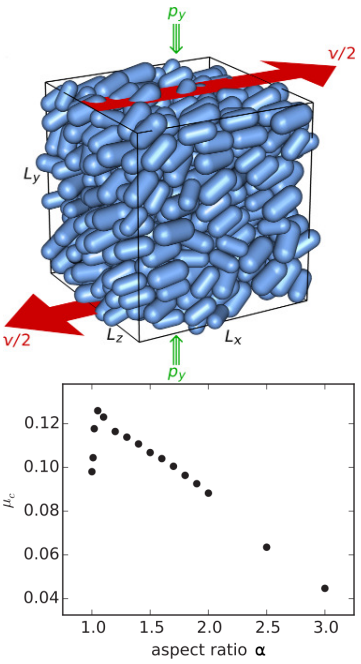

Simulation setup, and aspect ratio dependence of the effective friction coefficient

In our first investigation we performed 3D numerical simulations with *frictionless* spherocylinders. In homogenous shear flow we measured a number of rheological and static parameters, including the effective friction coefficient, first and second normal stress differences, volume fraction, coordination number, and orientation distribution; especially in the quasistatic limit. We found that the effective friction has a surprising behavior: in the quasistatic limit it is a nonmonotonic function of the aspect ratio α: from the spherical case $\alpha = 1$, it first sharply increases, reaches a maximum for $\alpha \approx 1.05$, and then gently decreases until $\alpha = 3$. We provided a microscopic interpretation for this unexpected behavior through the analysis of the distribution of dissipative contacts around the particles: as compared to spheres, slightly elongated grains enhance contacts in their central cylindrical band, whereas at larger aspect ratios particles tend to align and dissipate by preferential contacts at their hemispherical caps.
[Nagy et al., Phys. Rev. E (2017)]

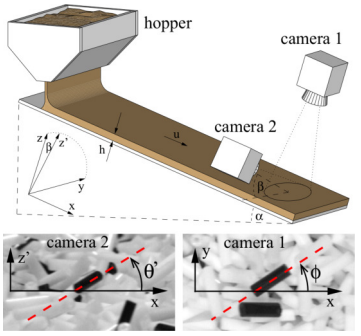

Experimental setup

We looked at similar systems in a different geometry: investigated the three-dimensional granular flow of elongated particles down an inclined plane, both numerically and experimentally. Similarly to sheared systems, the average particle orientation was found to enclose a small angle with the flow direction. In the bulk, this behavior is independent of the shear rate. At the surface, however, the particles move in more dilute conditions, and the average orientation strongly depends on the shear rate. A systematic numerical study varying the particle aspect ratio and the plane inclination reveals that the particle size perpendicular to the flow direction is an appropriate length scale to define an effective inertial number, which fully captures the impact of the particle shape on the system's rheology. Like in the case of spheres, density and friction result in well-defined functions of the effective inertial number, which was found to increase with particle aspect ratio. These inclined plane measurements – operating at high inertial numbers – complement our above results in homogenous shear flow, which is focused on small inertial numbers and the quasistatic limit.
[Hidalgo et al., Phys. Rev. Fluids (2018)]

We resolved the apparent disagreement between the above two results, in which in homogenous shear the effective friction was found to be a non-monotonic function of the aspect ratio (for frictionless spherocylinders in the quasistatic limit), while on an inclined plane it increases mono-

tonically (for frictional particles in rapid flow). We found that the key is the microscopic (particle) friction coefficient: as this quantity is increased, the locus of the maximum of the effective friction - inertial number curve shifts, and at values corresponding to typical, experimentally accessible granular materials the curve becomes monotonic. We revealed the microscopic origin of the peculiar non-monotonic behaviour for slippery particles: for small particle friction coefficient the increasing particle aspect ratio leads to stronger ordering and smaller average alignment angle – consequently less obstruction between particles – leading to less resistance against shearing. For particles with large surface friction, however, for increasing aspect ratio the stronger entanglement is not counteracted by the ordering as it is weaker in this case, leading to monotonically increasing shear resistance. We also showed the non-trivial dependence of the velocity fluctuations on the dominant dissipation mechanism, and traced back the behaviour of the normal stress differences to particle-level quantities.
[Nagy et al., New J. Phys. (2020)]

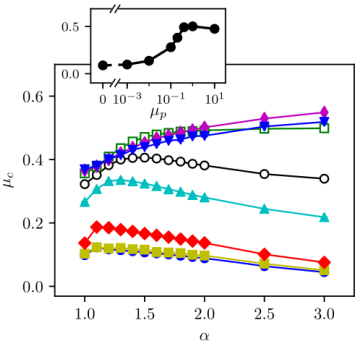

Aspect ratio dependence of the effective friction coefficient for frictional particles

Dense suspension of elongated particles

Shear induced ordering affects not only the rheology of dry granular assemblies, but also of suspensions. We modeled suspensions of neutrally buoyant elliptic particles immersed in a sheared fluid in 2D. The suspensions are characterized by the orientation distribution function that reflects shear induced rotation of the particles at low Reynolds numbers, and nearly stationary (swaying) particles at high Reynolds numbers. In both regimes the orientational ordering differs qualitatively from the behavior observed in the Stokesian-regime. The orientational distribution function becomes flatter with increasing packing fraction, as opposed to the sharpening previous work predicted in the Stokesian regime. At low particle concentrations the distribution differs significantly for the low Reynolds number and inertial regimes, whereas with increasing packing fraction convergence is observed. For dense suspensions, the particle–particle interactions dominate the particle motion, as can be seen in the strong orientational dependence of the pair correlation function.
[Tegze et al., Soft Matter (2020)]

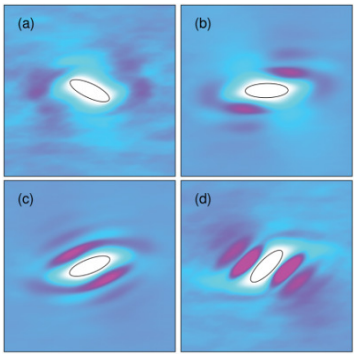

Pair correlation function at different orientations of the central particle

We investigated experimentally the rheological, viscoelastic and rheo-optical properties of a dispersion of non-spherical pigment particles at various volume fractions. We demonstrated that increasing volume fraction leads to a transition from a non-Newtonian flow behaviour to a viscoelastic response with a high storage modulus. A giant effective stress-optical coefficient was found (higher than in other reported cases), which is connected to the flow alignment of the elongated nanoparticles.
[Salamon et al., J. Molecular Liquids (2020)]

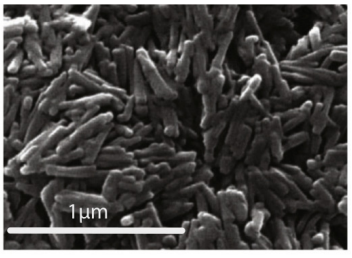

Scanning electron microscope image of pigment particles

General rheological properties

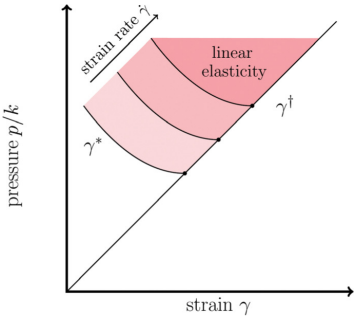

Linear elasticity window

Similarly to granular materials, the rheological behaviour of a large class of soft solids, including for example emulsions and foams, can be modeled with linear elasticity, provided the forcing is slow and weak. However, both of these approximations break down when the material loses rigidity such as near the jamming point. When deformations are too large, the material softens and eventually flows. Using computer simulations of athermal soft sphere packings we identified characteristic strain and time scales that quantify how and when the window of linear elasticity closes, and relate these scales to changes in the microscopic contact network. Our findings indicate that the mechanical response of jammed solids are generically nonlinear and rate-dependent on experimentally accessible strain and time scales.
[Boschan et al. Soft Matter (2016)]

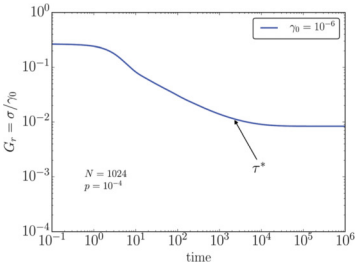

Time evolution of the shear modulus in response to step strain.

We also used numerical simulations to investigate the stress relaxation in athermal viscous soft spheres close to their unjamming transition. By systematically and simultaneously varying both the amplitude of the applied strain step and the pressure of the initial condition, we accessed both linear and nonlinear response regimes and controlled the distance to jamming. Stress relaxation in viscoelastic solids is characterized by a relaxation time, that separates short time scales, where viscous loss is substantial, from long time scales, where elastic storage dominates and the response is essentially quasistatic. We identified two distinct plateaus in the strain dependence of the relaxation time, one each in the linear and nonlinear regimes. The height of both plateaus scales as an inverse power law with the distance to jamming. By probing the time evolution of particle velocities during relaxation, we further identified a correlation between mechanical relaxation in the bulk and the degree of non-affinity in the particle velocities on the micro scale.
[Boschan et al., Soft Matter (2017)]

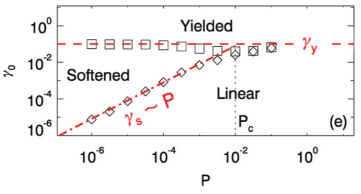

Linear, softened and yielded regimes

We developed a framework for softening and yielding of soft glassy materials, based on numerical simulations of oscillatory rheological tests. We showed that two distinct scenarios unfold depending on the material's packing density. For dense systems, there is a single, pressure-independent strain where the elastic modulus drops and the particle motion becomes diffusive. In contrast, for weakly jammed systems, a two-step process arises: at an intermediate softening strain, the elastic and loss moduli both drop down and then reach a new plateau value, whereas the particle motion becomes diffusive at the distinctly larger yield strain. We show that softening is associated with an extensive number of microscopic contact changes leading to a non-analytic rheological signature. Moreover, the scaling of the softening strain with pressure suggest the existence of a pressure scale above which softening and yielding coincide, and we verify the existence of this crossover scale numerically. Our findings thus evidence the existence of two distinct classes of soft glassy materials - jamming dominated and dense - and show how these can be distinguished by their rheological fingerprint.
[Dagois-Bohy et al., Soft Matter (2017)]

Granular flow in hopper (silo) geometry

We investigated experimentally the flow of practically frictionless materials using hydrogel particles. The softness of these particles adds qualitatively new features to the dynamics and to the character of the flow. We studied the outflow from a quasi-2D hopper, where we observed prominent features including intermittent clogs, peculiar flow fields in the container, and a pronounced dependence of the flow rate and clogging statistics on the container fill height. The latter is a consequence of the ineffectiveness of Janssen's law for low friction materials: the pressure at the bottom of a bin containing hydrogel spheres grows linearly with the fill height.
[Ashour et al., Phys. Rev. Fluids (2017)]

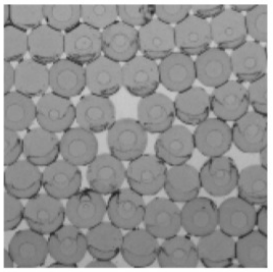

Broken hexagonal lattice of soft particles in quasi-2D hopper near the outlet

We investigated the outflow of hard grains from storage containers with narrow outlets, i.e. silos, by 3D (slow) X-ray computed tomography. Our focus was the comparison of flow of soft, highly deformable particles with low surface friction, and hard frictional grains. Soft grains behave qualitatively different in many respects, both in their static packing properties and during silo discharge. The local fill fraction of the soft grains depends upon the depth below the granular surface. The outflow of the soft hydrogel spheres involves the complete container volume with no stagnant zones; while for hard frictional grains the flow is concentrated in the middle part of the container.
[Stannarius et al., Granular Matter (2019)]

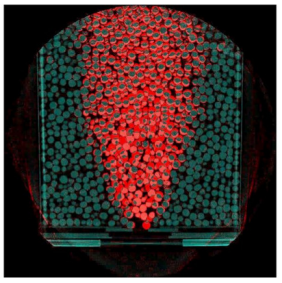

Image difference (red) before and after discharge, highlighting the flowing region of hard particles

We investigated the outflow of granular materials from silos also by 2D ultrafast x-ray computed tomography. The used acquisition speed of this tomograph is high enough to allow high-speed recording of two horizontal cross sections (each of them at a rate of 1000 images per second) of the container during the discharge of material. Analyzing space-time plots that were generated from the tomograms, we retrieved velocity profiles and packing structures in the container. We compared hard spherical grains with soft, low-friction hydrogel spheres, and found that their flow profiles are qualitatively different. While the hard spheres form stagnant zones at the container side walls, the hydrogel spheres with extremely low friction coefficient flow in all regions of the container. Moreover, a shell-like positional arrangement of the soft spheres induced by the container walls is revealed. The results obtained for the flow field structure confirm earlier conclusions drawn from sequences of x-ray tomograms of clogged states.
[Stannarius et al., New J. Phys. (2019)]

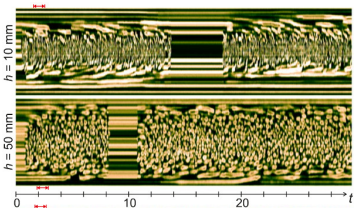

Space-time plots of cross sections with hard spheres at two different heights

We investigated experimentally the stationary flow field in a quasi-two-dimensional hopper. The behavior of six granular samples with different grain shapes (spherical, prolate, and oblate of varying aspect ratio) were compared. We showed that while the vertical velocity in the flowing region can be fitted with a Gaussian function for beads, in the case of elongated grains the flowing channel is narrower and is bordered with sharper velocity gradient. For elongated particles we quantified the deviations from the

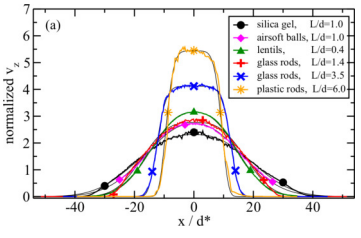

Vertical velocity profiles

Gaussian velocity profile. Focusing on the time evolution of the velocity profile, we found that the flow of elongated grains is characterized by velocity fluctuations of larger amplitude and lower frequency compared to the case of spheres.
[Szabó et al., Phys. Rev. E (2018)]

We investigated the particle stiffness dependence of granular flow out of a silo both experimentally and numerically. We showed that the particle stiffness has a strong effect on the qualitative features of silo discharge. For deformable grains, lowering the friction coefficient leads to a gradual change in the discharge curve: the flow rate becomes filling height dependent, it decreases during the discharge process. For hard grains the flow rate is much less sensitive to the value of the friction coefficient. We have analyzed the momentum balance in the region of the orifice (near the location of the outlet) for the case of soft particles with low friction coefficient, and proposed a phenomenological formulation that predicts the linear decrease of the flow rate with decreasing filling height, as well as viscous friction as dominant dissipation mechanism.
[Pongó et al., New J. Phys (2021)]

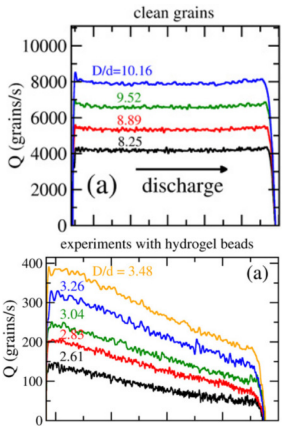

Silo discharge of hard and soft particles

After seeing that soft low friction particles and hard frictional particles have very different silo discharge properties, we were interested in which behaviour dominates in mixtures. Using experiments and numerical simulations we showed that the addition of small amounts, even as low as 5%, of hard grains to an ensemble of soft, low-friction grains already has significant consequences for a discharge of a 2-dimensional silo. The mixtures allow a direct comparison of the probabilities of the different types of particles to clog the orifice. We analyze these probabilities for the hard, frictional and the soft, slippery grains on the basis of their participation in the blocking arches, and compare outflow velocities and durations of non-permanent clogs for different compositions of the mixtures. Experimental results are compared with numerical simulations. The latter strongly suggest a significant influence of the inter-species particle friction.
[Wang et al., Soft Matter (2021)]

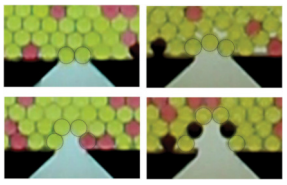

Blocking arches formed by 2, 3, 4 and 6 particles.

We studied numerically silo discharge for the case of a silo in which the bottom plate rotates with respect to the lateral wall. We found, in accordance with recent experimental findings, that depending on the size of the aperture D, two distinct behaviors emerge. For small orifices, the flow rate results in a strongly increasing function of the rotational frequency f. For large orifices however, the flow rate changes smoothly with f, denoting a slightly nonmonotonic behavior.
[Hernandez-Delfin et al., Phys. Rev. E (2020)]

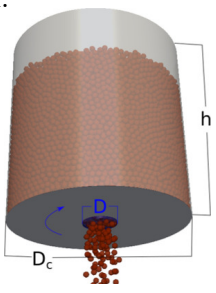

Setup with rotating bottom plate

In our final experiment in the hopper geometry we investigate the flow of elongated wooden pegs also with a rotating bottom plate. As for spherical grains, for small orifice sizes the rotating plate breaks clogs and results in an intermittent flow. However, instead of the power law dependence (Beverloo law) of spherical particles, for elongated particles the outflow displays an exponential dependence on the orifice diameter. Finite rotation of the bottom plate turns the discharge process from funnel flow to mass

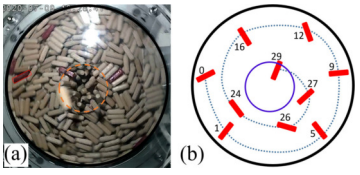

(a) Silo from its bottom, (b) trajectory of a tracer peg

flow because pegs at bottom are observed to move to the orifice and contribute to the total discharge current. While the current along the bottom slightly enhances the discharge rate in the intermittent flow regime, it reduces the discharge rate in the continuous flow (large orifice diameter) regime. We also examined the orientation of the pegs at the bottom, and observed shear-induced orientational ordering of the pegs at the bottom such that their long axes in average are oriented at a small angle to the motion of the bottom.
[To et al., Phys. Rev. E (2021)]

Inhomogenous shear flow

We studied the transition regime from quasi-static to dynamic shear regime using discrete element method (DEM) and by means of a mesoscopic model. We showed that at moderate shear rate multiple shear bands appear which eventually form a continuous shear profile for large shear rates. Both the model and the DEM simulations show a minimum in the shear stress and a maximum for the number of simultaneous shear bands, however the position of the two do not coincide. The scaling analysis of the kinetic energy indicated that the peak in the latter is the relevant parameter. We also showed how the long range order present in the quasi-static regime is gradually destroyed by the presence of multiple shear bands.
[Lévay et al., EPJ Web of Conf. (2017)]

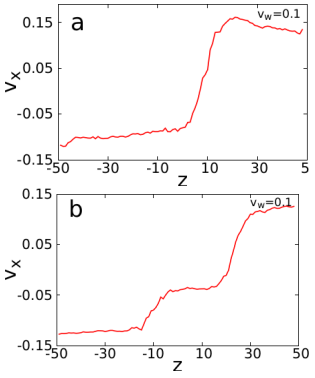

Velocity profiles displaying one and two shear bands

We investigated shear localization in a split-bottom Couette cell with smooth walls subject to a confining pressure both experimentally and numerically. We demonstrated how the characteristics of the shear zone evolve as the confining pressure and wall slip modify the local effective friction coefficient of the material. For increasing applied pressure, the shear zone evolves toward the center of the cylinder and grows wider and the angular velocity reduces compared to the driving rate of the bottom disk. We also varied systematically the ratio of the effective friction near the bottom plate and in the bulk in simulations and observed the resulting impact on the surface flow profile.
[Madani et al., Soft Matter (2021)]

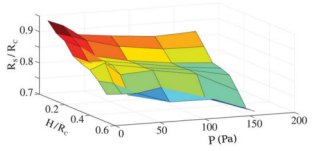

Shear zone position as a function of filling height and pressure

Particles of low symmetry

Particles of non-spherical shape, especially those with sharp corners, are often produced in fragmentation processes. We investigated theoretically and numerically the shape distribution of particle fragments. We have shown, using the theory of convex mosaics, that during binary fracture in 2D the average geometry has two attractors: quadrangles ("Platonic") and hexagons ("Voronoi"). In 3D the Platonic attractor is dominant: the average shape of natural rock fragments is indeed cuboid. Our simulations show that generic binary breakup drives all mosaics toward the Platonic attractor, explaining the ubiquity of cuboid averages. Deviations from binary fracture produce more exotic patterns, which are genetically linked to the formative stress field. We computed the universal pattern generator establishing

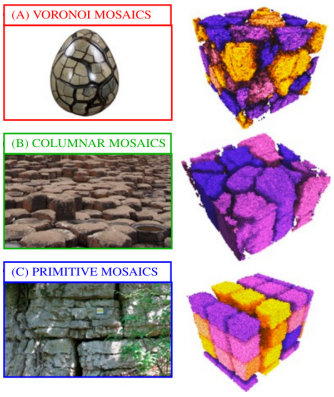

Field examples and simulations of 3D fracture patterns

this link, for 2D and 3D fragmentation.
This paper received over 700 international media mentions.
[Domokos et al., Proc. Natl. Acad. Sci. (2020)]

We investigated shear induced orientational ordering of asymmetric elongated particles experimentally. Corn grains and pegs with one end sharpened were studied using X-ray tomography during quasistatic shearing and silo discharge. We showed, that asymmetries can be detected in the orientational distributions of the particles, which are related to the modulated rotation of the particles during shear flow. Namely, when the particles rotate in a plane that is not horizontal, for energetic reasons they are expected to spend more time with the sharper (lighter) end pointing up. We quantified the resulting asymmetry of the orientational distribution in a split bottom Couette cell and in a silo discharge process.

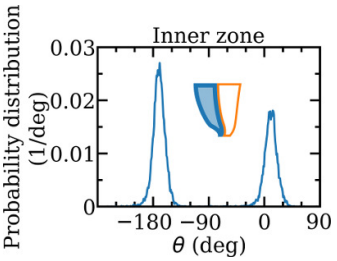

Asymmetric orientational distribution of sharpened pegs

[Nagy et al., manuscript (2021)] – *a copy of the manuscript is attached to the end of this report*

Secondary flow in granular systems

The flow of non-spherical granular particles produces a remarkable phenonemon: secondary flow – where a small velocity motion perpendicular to the direction of the external driving is generated. Since our results are not yet published, we present them in more detail here.

We observed earlier experimentally [Wortel, Börzsönyi, Somfai et al.; Soft Matter, 2015], that in a cylindrical split bottom shear cell particle accumulation ("heaping") occurs in the center of the cell. Later we confirmed using x-ray CT measurements, that this is a consequence of a slow radial drift of the particles, with average velocities 2-3 orders of magnitude smaller than the driving in the tangential direction. Heaping was observed most clearly for elongated particles; for spherical grains it is at least one order of magnitude weaker, or possibly even non-existent.

In this project we aimed to find the mechanism behind this secondary flow, so we turned to the simplest and analytically most managable case; initially leaving out details like strongly inhomogenous shear velocity field, inhomogenous pressure due to gravity, and curved streamlines. We have shown analytically, that under the $\mu(I)$ granular rheology if a homogenously sheared system is subjected to a small amplitude perturbation parallel to the streamlines, then vortices are generated with velocities perpendicular to the primary streamlines. The amplitude of the secondary flow (in first order in the perturbation) depends on rheological and geometrical factors, but most importantly it is proportional to the second normal stress difference (one of the difference between the diagonal elements of the stress tensor). We confirmed this result with particle-based numerical simulation of the same system.

According to the well established so called $\mu(I)$ rheology of granular systems [see for example Jop et al., Nature (2006)], under pressure isotropy the stress tensor σ_{ij} is related to the velocity field u by

$$\sigma_{ij} = p\left(\delta_{ij} + \mu(I)\frac{\dot{\gamma}_{ij}}{\dot{\gamma}}\right) ,$$

where $p = \frac{1}{3}\sigma_{ii}$ is the pressure, $\dot{\gamma}_{ij} = \dot{\Gamma}_{ij} + \dot{\Gamma}_{ji}$ is the shear rate with $\dot{\Gamma}_{ij} = \partial_i u_j$ and norm $\dot{\gamma}^2 = \frac{1}{2}\gamma_{ij}\gamma_{ij}$. The effective friction μ is a function of the dimensionless inertial number $I = \dot{\gamma}d/\sqrt{p/\rho}$, where d is the grain size and ρ the grain mass density. This differs significantly from the Newtonian fluid case, $\sigma_{ij} = p\delta_{ij} + \mu\dot{\gamma}_{ij}$, as for granular flow, due to the different dissipation mechanism, the shear (deviatory) stress is proportional to the pressure, and only weakly depends on the shear rate through $\mu(I)$.

We wish to extend this coordinate independent form to include dependence on nonzero normal stress differences, which in the standard notation used by the rheology community (x is the streamline, y is the velocity gradient, and z is the neutral or vorticity direction) reads $N_1 = \sigma_{xx} - \sigma_{yy}$ and $N_2 = \sigma_{yy} - \sigma_{zz}$. The simplest form satisfying expectable symmetry requirements is

$$\sigma_{ij} = p\left[\delta_{ij} + \mu(I)\frac{\dot\gamma_{ij}}{\dot\gamma} + \nu_1(I)\left(\frac{\dot\Gamma_{ki}\dot\Gamma_{kj}}{\dot\Gamma^2} - \tfrac{1}{3}\delta_{ij}\right) + \nu_2(I)\left(\frac{\dot\Gamma_{ik}\dot\Gamma_{jk}}{\dot\Gamma^2} - \tfrac{1}{3}\delta_{ij}\right)\right],$$

where the normal stress differences appear in the combinations

$$\nu_1 = \frac{N_1 + N_2}{p}, \qquad \nu_2 = \frac{N_2}{p}.$$

The base state is homogenous shear with linear velocity profile and reference shear rate $\dot\gamma_0$:

$$\boldsymbol{u}_0 = \begin{bmatrix}\dot\gamma_0 y\\ 0\\ 0\end{bmatrix}, \quad \dot{\boldsymbol{\Gamma}}_0 = \begin{bmatrix}0 & 0 & 0\\ \dot\gamma_0 & 0 & 0\\ 0 & 0 & 0\end{bmatrix}.$$

Assuming quastistatic limit, $I_0 = \dot\gamma_0 d/\sqrt{p_0/\rho} \ll 1$, the corresponding stress tensor reads:

$$\boldsymbol{\sigma}_0 = p_0\left(\pi_c\mathbf{1} + \begin{bmatrix}\nu_{1,c} & \mu_c & 0\\ \mu_c & \nu_{2,c} & 0\\ 0 & 0 & 0\end{bmatrix}\right) = p_0\left(\pi_c\mathbf{1} + \boldsymbol{\Sigma}_0\right),$$

where $\pi_c = 1 - \frac{1}{3}(\nu_{1,c} + \nu_{2,c})$, and where the subscripts 'c' indicate that μ, ν_1 and ν_2 are taken constants (independent of the shear rate) at their quasi-static values. We measured these quantities [Nagy et al., Phys. Rev. E (2017), Nagy et al., New J. Phys. (2020)], and found that for spherocylinders they are nonzero even in the quasistatic limit.

Assuming incompressibility, the mass and momentum conservation equations give

$$\begin{aligned}\partial_j u_j &= 0,\\ \rho\phi_c u_j\partial_j u_i &= \partial_j\sigma_{ij} + b_i\,,\end{aligned}$$

where b_i is an external body force. We take it as an infinitesimal perturbation exclusively in the x direction:

$$\boldsymbol{b} = \epsilon\frac{p_0}{d}\begin{bmatrix}f(y,z)\\ 0\\ 0\end{bmatrix},$$

where ϵ is its vanishing dimensionless amplitude, and f its normalised profile in the (y,z)-plane.

Assuming that $\epsilon \ll 1$, the response of the velocity and pressure to this perturbation can be written at the linear order as (exploiting invariance in x direction):

$$\boldsymbol{u} = \boldsymbol{u}_0 + \epsilon\dot\gamma_0 d\begin{bmatrix}U_x(y,z)\\ U_y(y,z)\\ U_z(y,z)\end{bmatrix} + o(\epsilon^2), \qquad p = p_0\left(1 + \epsilon P(y,z)\right) + o(\epsilon^2),$$

where U_i and P are unknown function we wish to relate to f.

We calculated up to linear order in terms of these functions the shear rate $\dot\gamma_{ij}$ and its norms $\dot\gamma$ and $\dot\Gamma$, then the stress tensor; these lead to complicated but manageable expressions which we omit here. Writing these back to the mass and momentum conservation equations lead to

$$\begin{aligned}\partial_y U_y + \partial_z U_z &= 0,\\ 0 &= \partial_y P + d\partial_{zz}U_x + \tfrac{1}{\mu_c d}f,\\ -\mu_c d(\partial_{zz}U_y + \partial_{yy}U_y) &= \pi_c\partial_y P - \tfrac{\nu_{2,c}}{\mu_c d}f,\\ -\mu_c(\partial_{zz}U_z + \partial_{yy}U_z) &= \nu_{2,c}\partial_{yz}U_x\,,\end{aligned} \tag{1}$$

which describe the response of the granular shear flow to an x-directional perturbation up to linear order.

As a concrete example, for a simple sinusoidal perturbation

$$f(y,z) = \sin(k_y y/d)\cos(k_z z/d)\,,$$

the response can be written in the form

$$\begin{aligned} U_x &= a_x \sin(k_y y/d)\cos(k_z z/d), \\ U_y &= a_y \sin(k_y y/d)\cos(k_z z/d), \\ U_z &= a_z \cos(k_y y/d)\sin(k_z z/d), \\ P &= a_p \cos(k_y y/d)\cos(k_z z/d), \end{aligned}$$

where the amplitudes are restricted by Equations (1) to

$$\begin{aligned} a_x &= \frac{\pi_c + \nu_{2,c}}{k_z^2 \mu_c(\pi_c - \nu_{2,c})}, \\ a_y &= \frac{\nu_{2,c}(\pi_c + \nu_{2,c})}{(k_y^2 + k_z^2)\mu_c^2(\pi_c - \nu_{2,c})}, \\ a_z &= -\frac{k_y \nu_{2,c}(\pi_c + \nu_{2,c})}{k_z(k_y^2 + k_z^2)\mu_c^2(\pi_c - \nu_{2,c})}, \\ a_p &= -\frac{2\nu_{2,c}}{k_y \mu_c(\pi_c - \nu_{2,c})}. \end{aligned}$$

We stress here that the amplitudes a_y and a_z, which are related to the perpendicular flow, are nonzero, and are proportional to the second normal stress difference through $\nu_{2,c}$.

The velocity field in the (y,z) plane is displayed in the figure below, together with its numerical simulation counterpart (obtained at small perturbation amplitude and averaged over long time interval). The numerical results confirm the analytical calculations, even though the simulations contain inherent noise due to the interactions of the particles.

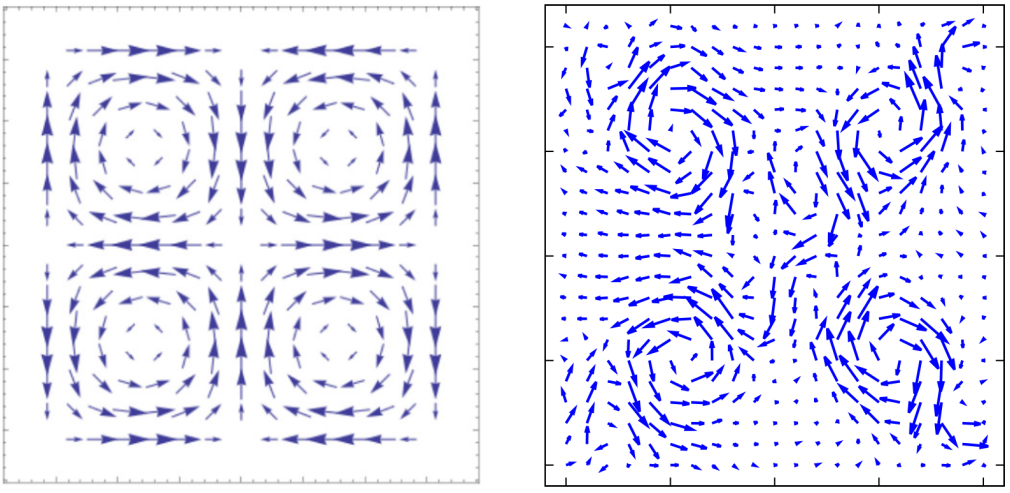

Velocity field perpendicular to the streamlines: (left) analytical, and (right) numerical.

In summary, we have shown both analytically and numerically that in homogenous granular shear flow a streamline-oriented perturbation can generate perpendicular, secondary flow, with amplitude proportional to the second normal stress difference. This mechanism is responsible for heaping, where the streamline-oriented perturbation is replaced by inhomogenous shear rate

(but which is still invariant in the streamline direction). This phenomenon resembles, but is distinct from the Weissenberg-effect (or rod climbing) of viscoelastic materials.

Statistical mechanics of granular packings

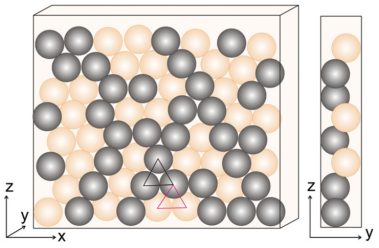

Front and side view of the setup

The packing of arbitrary shaped particles is an intricate problem; to make progress we took a step back and considered sphere packings, which turned out to be related to fundamental statistical physics models. The optimal packings of monodisperse spheres are solved problems in two and three dimensions. The main difference between them is that the two-dimensional ground state can be easily achieved by simple dynamical processes, while in three dimensions this is impossible due to the difference in the local and global optimal packings. We have shown experimentally and numerically that in $2+\epsilon$ dimensions, realized by a container which is in one dimension slightly wider than the spheres, the particles organize themselves in a triangular lattice, while touching either the front or rear side of the container. If these positions are denoted by "up" and "down", the packing problem can be mapped to a 1/2 spin system. At first it looks frustrated with spin-glass like configurations, but the system has a well defined ground state built up from isosceles triangles. When the system is agitated, it evolves very slowly towards the potential energy minimum through metastable states. We show that the dynamics is local and is driven by the optimization of the volumes of 7-particle configurations and by the vertical interaction between touching spheres.
[Lévay et al., Soft Matter (2018)]

We used the above $2+\epsilon$ dimensional system to test the so-called Edwards theory of granular assemblies. This framework, dating back to about 3 decades, describes the statistics of granular packings by an ensemble of equiprobable jammed states, where in analogy to equilibrium statistical mechanics the free energy is replaced by the available volume of the particles. Experimental tests of this model remained scarce so far. Our system evolves toward a ground state, but due to incompatible domain structures it gets trapped. Analytical calculations reproduce relatively well our simulation results, which allows us to test Edwards theory on a coupled system of two subsystems with different properties. We found that the joint system can only be described by the Edwards theory if considered as a single system due to the constraints in the stresses. The results show counterintuitive effects as in the coupled system the change in the order parameter is opposite to what is expected from the change in the compactivity.
[Lévay et al., Phys. Rev. E (2021)]

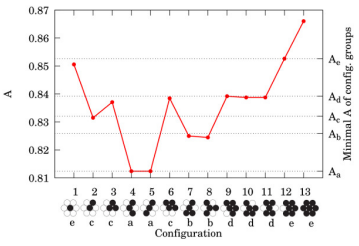

The local configurations and the available area of the central particle

Appendix: near final version of [Nagy et al., manuscript (2021)]

Flow of asymmetric elongated particles

Viktor Nagy[1], Fan Bo[1], Ellák Somfai[1], Ralf Stannarius[2] and Tamás Börzsönyi[1*]

[1]Wigner Research Centre for Physics, Budapest, Hungary.
[2]Otto von Guericke University, Magdeburg, Germany.

*Corresponding author(s). E-mail(s): borzsonyi.tamas@wigner.hu;
Contributing authors: nagyviktor2@gmail.com; fan.bo@wigner.hu;
somfai.ellak@wigner.hu; ralf.stannarius@ovgu.de;

Abstract

Shear induced orientational ordering of asymmetric elongated particles is investigated experimentally. Corn grains and pegs with one end sharpened are studied using X-ray tomography (X-ray CT) during quasistatic shearing and silo discharge. We show, that asymmetries can be detected in the orientational distributions of the particles, which are related to the modulated rotation of the particles during shear flow. Namely, when the particles rotate in a plane that is not horizontal, for energetic reasons they are expected to spend more time with the sharper (lighter) end pointing up. We quantify the resulting asymmetry of the orientational distribution in a split bottom Couette cell and in a silo discharge process.

Keywords: granular flow, shear flow, silo flow, elongated particles

1 Introduction

When a granular material consisting of elongated particles is subjected to shear, the particles perform a rotating motion. Their rotation has a noisy character due to the interaction with neighbouring particles. The ensemble averaged rotation velocity however shows a clear angle dependence: it is larger when the particle is oriented with its long axis parallel to the flow gradient (i.e. perpendicular to the flow), and smaller when the particle is nearly parallel to the flow direction. This results in an average alignment of the grains nearly

parallel to the flow, as they spend the longest time around that orientation [1–4]. Thus measuring the orientation distribution of the grains from a snapshot during flow, one can get information on the behaviour of particles in a sheared system, even if the dynamics of individually rotating grains is not tracked.

Several works have shown that for elongated or flat particles increasing shape anisotropy of the grains leads to stronger orientational ordering, higher effective friction of the sample or stronger shear banding [1, 5–10]. For particles with low interparticle friction ($\mu_p \leq 0.4$ in 3D and $\mu_p \leq 0.15$ in 2D) an interesting non-monotonic dependence of the effective friction was found as a function of grain elongation [5, 7]. The effect of grain shape on the flow field in a silo, the discharge rate and clogging probability was also investigated [11–20]. The flow field was found to be more concentrated to the silo center, with larger temporal fluctuations for more elongated grains [18–20]. Even if some of the above investigations involved asymmetric elongated grains (e.g. corn seeds) [17, 18], the role of grain shape asymmetry is not well explored in shear flow or silo flow.

2 Experimental system

In this work two experimental geometries have been employed to study the flow of a granular assembly of elongated asymmetric particles. In the first experiment the granular material was exposed to shear in the so called cylindrical split-bottom shear cell (see Fig. 1(a)). In this device the central part of the granular sample is rotated, while the outer part of the sample is not moving. The sheared region is in between the moving and standing parts, with the highest shear rate in the middle of this region. We define the core of the shear zone as the region where the time averaged rotation rate is in between 5% and 95% of the rotation rate of the inner part. This shear zone core is indicated with red contours and white particles in Fig. 1(a). The radius of the cell was 28.5 cm, the radius of the rotating plate was 19.5 cm, while the thickness of the granular layer was 6 cm. Before recording the data the sample was presheared with 15 full rotations in order to eliminate any transient effects and to ensure stationary shear throughout the experiment. During the experiment quasistatic shearing was applied which was stopped at regular intervals of 360° of rotation of the inner part, and then a pair of X-ray tomograms (CT) was taken of the sample. The plate was rotated by a small amount (2°) between the two tomograms, with the aim of enabling the detection of particle displacements for the determination of the flow field. We recorded 50 pairs of tomograms for sharpened pegs and 19 pairs of tomograms for corn seeds. In the second experiment the granular material was discharged from a nearly cylindrical silo with a circular orifice at the bottom (Fig. 1(b)). The diameter of the orifice was relatively small so that the flow often clogged. Each clogged configuration was recorded with X-ray CT. We recorded 109 tomograms for sharpened pegs and 30 tomograms for corn seeds. The container had a height of 21.4 cm and a diameter of 19 cm. The tomograms for both experiments were

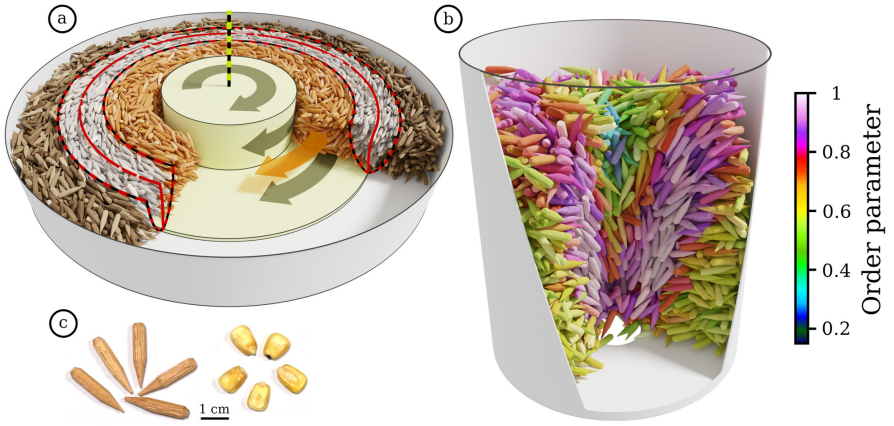

Fig. 1 Sketches of the experimental configurations: (a) cylindrical split-bottom shear cell (b) silo. Both pictures include grains as detected in tomograms. In panel (a) the shear zone is indicated with red lines, while particles in the shear zone are colored white. In panel (b) particle colors represent the local order parameter, according to the colorbar next to the cylinder. (c) Photographs of the samples: sharpened pegs and corn seeds.

obtained with the Siemens Artis zeego X-ray Tomograph of the STIMULATE-lab of the Otto von Guericke University in Magdeburg. The recorded volume was 25.2 cm × 25.2 cm × 19 cm, with a spatial resolution of 2.03 pixel/mm, resulting in tomograms of 512 × 512 × 386 pixels. The recording time of a tomogram was about 2 minutes.

Two types of particles were used in the experiments: sharpened pegs and corn seeds. In addition to being elongated both particles are asymmetric in the sense that the two ends are different: the corn seeds have a wedge shape, while for the pegs one of the ends is sharpened (see the photographs in Fig. 1(c)). The pegs had a diameter of $d = 5$ mm and a length of $L = 25$ mm, while the typical dimensions of the corn seeds were about $d_1 = 5$ mm, $d_2 = 8$ mm, and $L = 12$ mm. A self developed particle identification code was used to detect the grains. The pictures on Fig. 1(a)-(b) show reconstructed pegs from actual measurements. In the shear cell (Fig. 1(a)) the particles are colored according to their location in order to visualize the core of the shear zone. In the silo (Fig. 1(b)) the colors represent the local orientational order parameter.

3 Results and Discussion

3.1 Shear flow

In the first experiment, we characterize the flow field and the orientation of the particles in stationary shear flow in the split bottom shear cell. Fig. 2 indicates the main features of the velocity field in this system: the flow velocity is tangential, while the velocity gradient is nearly horizontal. The side view in Fig. 2(b) shows that the lines parallel to the local velocity gradient are

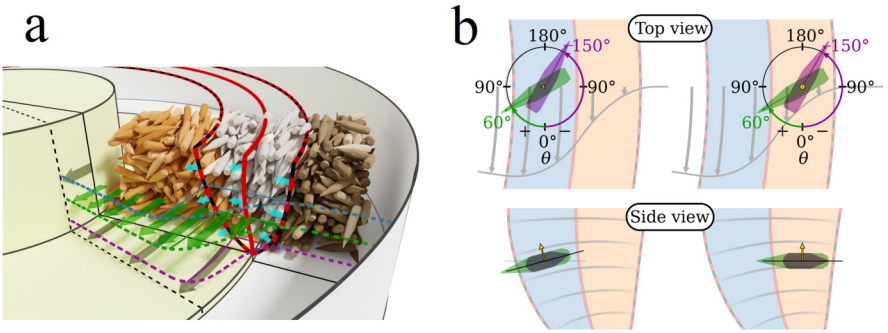

Fig. 2 Geometry of the shear flow in a cylindrical split bottom cell. In panel (a) the contours and the middle of the shear zone are indicated with red lines, the particles in the shear zone are colored white. The velocity profiles at three different heights are indicated with three different colors, the green arrows indicate the velocity profile in the middle of the granular layer. In panel (b) a top view and a side view of the shear zone is sketched. On the top view the flow velocity is indicated with arrows. On the side view the direction of the local velocity gradient is indicated with lines: it is nearly horizontal in the outer half of the shear zone (orange) and slightly tilted in the inner part of the shear zone (light blue). Two particles lying in the shear plane with orientation angles $\theta = -150°$ and $\theta = 60°$ are shown as examples.

somewhat curved. This results in a practically horizontal velocity gradient in the outer half of the shear zone core (indicated with orange) and a slightly tilted velocity gradient in the inner half of the shear zone core (indicated with light blue). As discussed in earlier works [1–4], elongated particles in a shear flow get oriented with their long axis parallel (or nearly parallel) to the shear plane (spanned by the flow velocity and velocity gradient). They perform a rotation within the shear plane with a fluctuating rotation velocity which depends on the actual interactions with neighbours. The ensemble averaged rotation velocity however shows a clear orientation dependence: particles with their long axis nearly parallel to the flow rotate slower than those perpendicular to the flow. This results in orientational ordering with an average alignment of the grains nearly parallel to the main flow.

As a first step, we consider the particles as simple elongated grains (i.e. in the first approximation we forget about the difference between the non-sharpened and sharpened ends) and characterize the shear induced alignment by a nematic order parameter S, which is the largest eigenvalue of the orientation tensor [1, 2]. Random grain orientations would lead to $S = 0$, while $S = 1$ corresponds to a perfect alignment with all grains parallel to each other. Figs. 3(a) and (d) show the maps of the order parameter S, while Figs. 3(b) and (e) show the maps of the average alignment angle for sharpened pegs and corn seeds, respectively. The maps show a vertical cross section of the cell with the data averaged in the azimuthal direction. These figures clearly show, that both systems get aligned in the sheared region, with the strongest alignment in the core of the shear zone. The order parameter reaches a larger value for sharpened pegs than for the less elongated corn seeds. The alignment angle is

slightly smaller for sharpened pegs than for corn seeds. All this is in accordance with earlier observations on normal (not sharpened) pegs and and rice particles [1, 2].

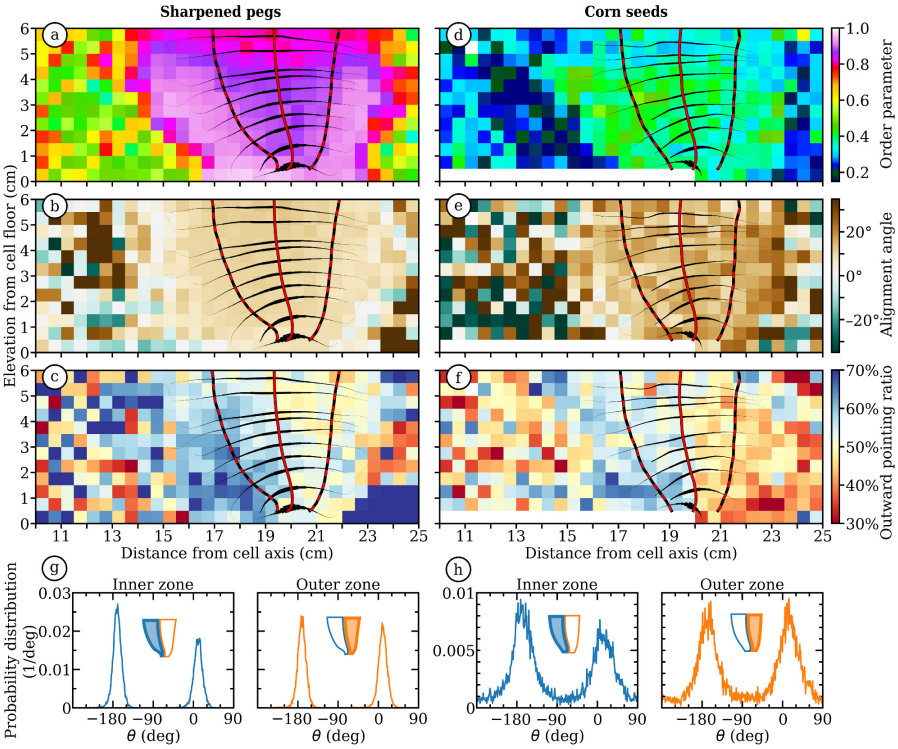

Fig. 3 Maps of the orientational order parameter (row 1), average alignment angle (row 2) ratio of outward pointing particles (row 3) and the distributions of particle orientations (row 4) for sharpened pegs (left) and corn seeds (right) in the cylindrical split-bottom shear cell.

As a second step, we determine the orientation distribution of the particles by fully considering their asymmetric shape (i.e. taking into account the difference between their two ends). Figs. 3(g)-(h) show the distribution of the orientation angle θ, defined as the angle between the long axis of the particle and the flow direction as shown in Fig. 2(b) (top view). The orientation distribution is separately shown in the outer and inner half of the core of the shear zone for both grain types: sharpened pegs and corn. The distributions have narrower peaks for pegs, i.e. shear induced ordering is stronger for longer grains, and the peaks are slightly shifted with respect to the flow direction (0^o and 180^o), in accordance with earlier observations on other elongated particles [1, 2]. Interestingly, in the outer half of the shear zone core the peaks are symmetric, while in the inner half of the shear zone core they are asymmetric. As discussed above the shear gradient is nearly horizontal in the outer half, while

it is slightly tilted in the inner half. Thus the deviation from the flow direction has a vertical component in the inner half, while it is nearly horizontal in the outer half. The asymmetry of the distributions in the inner half means, that there is a slightly higher probability to find grains with their sharper end pointing outwards than inwards. This can be explained by the fact, that the two configurations are energetically different, since outward pointing grains have their thicker end at a lower position, while inward pointing grains have their thicker end at a higher position (see the two grains presented as examples in Fig. 2(b) on the left side of the side view). For horizontal shear gradient there is no such difference (see the two grains on the right side of the side view), so the distributions in the outer half of the zone (see again Figs. 3(g)-(h)) are nearly symmetric.

The maps of the outward pointing ratio thus nicely visualize this asymmetry throughout the whole cell (Figs. 3(c)-(f)). The asymmetry is more pronounced towards the inner side of the shear zone (blue colors) and is larger for the case of sharpened pegs than for corn seeds.

3.2 Clogging in a silo

In the second experiment, we investigate the grain orientations during the discharge of a nearly cylindrical silo with a circular orifice at the bottom. The size of the orifice was relatively small: $D = 3.3$ cm for sharpened pegs, and $D = 2.6$, 2.8 and 3.0 cm for corn seeds. This ensured frequent clogs during the discharge process. A typical avalanche size between two subsequent clogs corresponds to a handful of grains. A tomogram was recorded of each clogged configuration. During the avalanches the grains sink towards the orifice in a cone shaped region, while other grains in a stagnant zone near the silo wall do not move. The region with the strongest shear is nicely visualized by the shear induced orientational ordering of the grains, see the region with pink color in Fig. 1(b). Grains in the stagnant zone (outside of the shear zone) are mostly horizontal, as they keep their orientation obtained during the filling procedure. Our goal is to determine the particle orientations in the sheared region.

In order to identify the sheared region of our granular sample in the silo, we plot the map of the orientational order parameter in a vertical cross section of the silo (see Figs. 4(b)-(c)) by averaging the data in the azimuthal direction. As we see, orientational ordering is observed in a tilted region with a much larger order parameter for sharpened pegs than for corn seeds. This is similar to the observations in the split bottom shear cell described above. In the following we analyze particle orientations in the regions in between the dashed lines in Figs. 4(b)-(c), looking for differences between the orifice region (where the clog occurs) and above. In Figs. 4(a)-(d) we quanify the orientation of the particle long axis with respect to the streamline by showing the value of the component parallel to the streamlines as a function of the particles distance from the dome, which forms the clog above the silo outlet. In order to define the position of the dome we first order the particles as a function of the distance between their centers of mass and the apex of the cone corresponding to the flowing

region, i.e. the lower dashed line. The position of the dome is then defined by

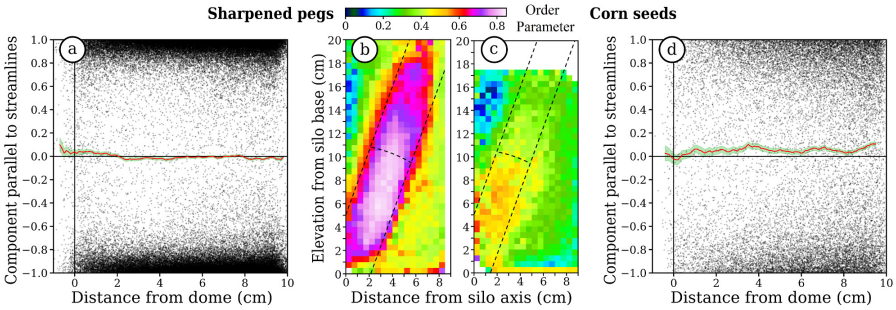

Fig. 4 Grain orientation data for (a)-(b) sharpened pegs and (c)-(d) corn seeds in the silo. Panels (a) and (d) quantify the orientation of the particle long axis with respect to the streamline, by showing the value of the component parallel to the streamlines as a function of the particles distance from the dome which forms the clog above the silo outlet. Panels (b) and (c) show the maps of the orientational order parameter.

the center of mass of particle No. 5, i.e. on each tomogram the centers of mass of 4 particles fall below the dome, particle No. 5 is on the dome, and all the other particles are above the dome. The component parallel to the streamlines is positive when the sharper end of the particle points away the orifice and it is negative when it points towards from the orifice. In Figs. 4(a) and (d) we see two clouds of points, one on the positive and one on the negative side of the graph. These clouds indicate the orientational ordering of the grains, and show stronger ordering for sharpened pegs than for corn seeds. The balance between the two clouds is visualized by the red data curve. Red data points above zero mean more particles pointing up (i.e. away from the orifice) than down. As we see, for corn seeds the balance is slightly positive above the dome, but is around zero near the dome. This means that above the dome the wedge shaped corn seeds slightly favour the "sharp end up" configuration against the "sharp end down" configuration, while in the dome, where the clog is formed, this difference seems to disappear. This is coherent with the argument, that a dome forms more easily with wedge shaped particles pointing down. The scenario is different for the case of sharpened pegs. There, the balance is practically zero above the dome, meaning equal number of "sharp end up" and "sharp end down" particles. Near the dome however, the balance becomes slightly positive, meaning slightly more "sharp end up" particles. Although the difference between the case of sharpened pegs and corn seeds is very small, it indicates that the particle configurations and the mechanism for clog formation might be a slightly different for these two particles.

4 Conclusion

Our experimental observations on the flow of asymmetric elongated particles in a sheared system or during silo discharge show, that for the case of corn shaped

grains or pegs shapened at one end one can detect the effect of the particle asymmetry on the shear induced orientational ordering process. Namely, elongated grains in general rotate in a shear flow with modulated rotation velocity: faster rotation when perpendicular to the flow and slowing down when their orientation is near the flow direction. This leads to orientational ordering, as grains spend more time with their long axis oriented near the flow direction. This dynamics is slightly modified for asymmetric particles: if their plane of rotation is not perpendicular to gravity they are expected to spend more time in the "sharper end up" than in the "sharper end down" configuration, so the orientational distribution is expected to become asymmetric. We experimentally detect this asymmetry in the particle orientations in a cylindrical split bottom shear cell for both corn seeds and sharpened pegs. For the case of silo discharge the asymmetry is detected in most of the sheared region for corn seeds, except in the vicinity of the orifice. For sharpened pegs the asymmetry only appears in the orifice region with a very small amplitude. This indicates, that in the silo the clog formation mechanism also influences the particle orientation near the orifice. Future numerical simulations might help to get more insight into the processes leading to the asymmetric orientational distributions observed in our experiments.

Acknowledgments. Financial support by the European Union's Horizon 2020 Marie Skłodowska-Curie grant "CALIPER" (No. 812638), by the Hungarian National Research, Development and Innovation Office – NKFIH (Grant No. OTKA K 116036), by the DAAD/TKA researcher exchange program (Grant No. 274464) are acknowledged. The authors thank G. Rose for providing access to the X-ray CT facility and B. Szabó for technical assistance. B. F. and T.B appreciate discussions with J. Dijksman and J. van der Gucht.

References

[1] Börzsönyi, T., Szabó, B., Törös, G., Wegner, S., Török, J., Somfai, E., Bien, T., and Stannarius R.: Orientational order and alignment of elongated particles induced by shear. Phys. Rev. Lett. **108**, 228302 (2012)

[2] Börzsönyi, T., Szabó, B., Wegner, S., Harth, K., Török, J., Somfai, E., Bien, T., and Stannarius R.: Shear induced alignment and dynamics of elongated granular particles. Phys. Rev. E **86**, 051304 (2012)

[3] Börzsönyi, T. and R. Stannarius: Granular materials composed of shape-anisotropic grains. (Review article) Soft Matter **9**, 7401 (2013)

[4] Wegner, A., Börzsönyi, T., Bien, T., Rose, G., and Stannarius, R.: Alignment and dynamics of elongated cylinders under shear. Soft Matter **8**, 10950 (2012)

[5] Nagy, D.B., Claudin, P., Börzsönyi, T., and Somfai, E.: Flow and rheology of frictional elongated grains New. Journal of Physics **22**, 073008 (2020)

[6] Hidalgo, R.C., Szabó, B., Gillemot, K., Börzsönyi, T., and Weinhart, T.: Rheological response of non-spherical granular flows down an incline. Phys. Rev. Fluids **3**, 074301 (2018)

[7] Trulsson, M.: Rheology and shear jamming of frictional ellipses. J. Fluid Mech. **849**, 718 (2018)

[8] Marschall, T.A., Teitel, S.: Athermal shearing of frictionless cross-shaped particles of varying aspect ratio. Granular Matter **22**, 4 (2020)

[9] Boton, M., Azéma, E., Estrada, N., Radjai, F. and Lizcano, A.: Quasistatic rheology and microstructural description of sheared granular materials composed of platy particles. Phys. Rev. E **87**, 032206 (2013)

[10] Nouguier-Lehon, C.: Effect of the grain elongation on the behaviour of granular materials in biaxial compression Comptes Rendus Mecanique **338**, 587 (2010)

[11] Cleary, P.W.: The effect of particle shape on hopper discharge. Second International Conf. on CFD in the Minerals and Process Industries pp 71–6 (1999)

[12] Cleary, P.W., and Sawley, M.L.: DEM modelling of industrial granular flows: 3d case studies and the effect of particle shape on hopper discharge. Appl. Math. Modelling 26 89–111 (2002)

[13] Liu, S.D., Zhou, Z.Y., Zou, R.P., Pinson, D. and Yu, A.B., Flow characteristics and discharge rate of ellipsoidal particles in a flat bottom hopper. Powder Technol. **253**, 70 (2014)

[14] Li, J., Langston, P.A., Webb, C. and Dyakowski, T.: Flow of sphero-disc particles in rectangular hoppers- a DEM and experimental comparison in 3d. Chem. Eng. Sci. **59**, 5917 (2004)

[15] Langston, P.A., Al-Awamleh, M.A., Fraige, F.Y. and Asmar, B.N.: Distinct element modelling of non-spherical frictionless particle flow Chem. Eng. Sci. **59** 425 (2004)

[16] Ashour, A., Wegner, S., Trittel, T., Börzsönyi, T., and Stannarius, R.: Outflow and clogging of shape-anisotropic grains in hoppers with small apertures Soft Matter **13**, 402 (2017)

[17] Escudero, F., Olivares, M.C.V, Unac, R., Vidales, A.M., and Benito, J.: Silo discharge: influence of the particle shape on the velocity profiles. EPJ Web of Conferences 249, 03029 (2021)

[18] Tao, H., Jin, B., Zhong, W., Wang, X., Ren, B., Zhang, Y., Xiao, R.: Discrete element method modeling of non-spherical granular flow in rectangular hopper. Chem. Eng. Proc. **49**, 151 (2010)

[19] Markauskas, D., Kacianauskas, R.: Investigation of rice grain flow by multi-sphere particle model with rolling resistance. Granular Matter **13**, 143 (2011)

[20] Szabó, B., Kovács, Zs., Wegner, S., Ashour, A., Fischer, D., Stannarius, R. Börzsönyi, T.: Flow of anisometric particles in a quesi-two-dimensional hopper. Phys. Rev. E **97**, 062904 (2018)

[21] Börzsönyi, T., Somfai, E., Szabó, B., Wegner, S., Mier, P., Rose, G., and Stannarius R.: Packing, alignment and flow of shape-anisotropic grains in a 3D silo experiment. New J. Phys. **18**, 093017 (2016)